PCCP

ROYAL SOCIETY OF CHEMISTRY

PAPER

View Article Online
View Journal | View Issue

Cite this: *Phys. Chem. Chem. Phys.*, 2021, **23**, 15209

Ligated aluminum cluster anions, LAl_n^- (n = 1–14, L = $N[Si(Me)_3]_2$)

Gaoxiang Liu, †[a] Sandra M. Ciborowski, [a] Georgia R. Montone,[b] William H. Sawyer,[b] Boggavarapu Kiran,[c] Anil K. Kandalam *[b] and Kit H. Bowen*[a]

Received 7th March 2021,
Accepted 29th June 2021

DOI: 10.1039/d1cp01020d

rsc.li/pccp

A wide range of low oxidation state aluminum-containing cluster anions, LAl_n^- (n = 1–14, L = $N[Si(Me)_3]_2$), were produced *via* reactions between aluminum cluster anions and hexamethyldisilazane (HMDS). These clusters were identified by mass spectrometry, with a few of them (n = 4, 6, and 7) further characterized by a synergy of anion photoelectron spectroscopy and density functional theory (DFT) based calculations. As compared to a previously reported method which reacts anionic aluminum hydrides with ligands, the direct reactions between aluminum cluster anions and ligands promise a more general synthetic scheme for preparing low oxidation state, ligated aluminum clusters over a large size range. Computations revealed structures in which a methyl-group of the ligand migrated onto the surface of the metal cluster, thereby resulting in "two metal-atom" insertion between Si–CH_3 bond.

Introduction

In recent years, aluminum chemistry has flourished as a result of the major progress in the research on aluminum's low oxidation states (OS).[1,2] These studies started by the advent of low OS aluminum precursors such as AlX (X = Cl, Br, I, Cp*)[3–8] and largely advanced by utilizing various organic ligands to protect the low OS aluminum compounds.[9–31] Among these ligands, deprotonated pentamethylcyclopentadiene (Cp*) and deprotonated hexamethyldisilazane (HMDS) received special attention.[9–12,17–31] Cp* has been reported to protect low OS aluminum compounds of various structures, such as rings and cages,[24–27] and of various stoichiometries, including either aluminum-poor or aluminum-rich clusters.[29–31] The other ligand, deprotonated HMDS, $N[Si(Me)_3]_2$, which is isovalent to NH_2^- and large in size, has also been widely used to protect the central aluminum cluster cores from outer environments. For example, cluster-like Al_7, Al_{12}, Al_{69}, and Al_{77}[9–12] with different numbers of $N[Si(Me)_3]_2$ as protective ligands were synthesized using various Al*X* precursors. Studying such clusters can provide insights into the crossover between the molecular species and the bulk metal for main-group elements.[12]

Recently, we extended the study of Cp*- and deprotonated HMDS-ligated aluminum clusters into the gas phase by exploring the reactions between aluminum hydride cluster anions $Al_xH_y^-$ and Cp*H or HMDS. The formation of and the anion photoelectron spectra of several previously unknown cluster anions, $Cp^*Al_nH^-$ (n = 1–3)[32] and LAl_n^- (n = 2–4, L= $N[Si(Me)_3]_2$),[33] were reported. In these studies, the precursors $Al_xH_y^-$ were generated by a pulsed-arc cluster ion source (PACIS)[34] and then allowed to drift into a beam-gas reaction cell[35] to react with the ligand (Cp*H or HMDS). The accompanying density functional theory (DFT) based calculations of neutral and anionic LAlH and LAl_n (n = 2–4) revealed few distinct structural features: (i) the lowest energy isomers were dominated by structures in which the Si–C bond of the ligand molecule was activated by the Al_n cluster, resulting in at least one aluminum atom being inserted into one of the Si–CH_3 bonds of the ligand. (ii) As the number of aluminum atoms increased from n = 2 to n = 4, the additional aluminum atoms preferred to maximize Al–Al interactions by adding peripherally to the existing Al atoms of the smaller systems, *i.e.*, LAl_{n-1}. In addition, our measured and calculated vertical detachment energies (VDE) of the ligated-Al_n^- clusters[33] were identical to those of their pure Al_n^- counterparts.[36–38]

In the present work, we adopted a different strategy to generate ligated aluminum clusters in the gas phase: we used a laser vaporization source to make bare aluminum cluster anions Al_n^-, and reacted them with HMDS in a reaction cell. Ligated aluminum cluster anions LAl_n^- (L = $N[Si(Me)_3]_2$), where n ranges from 1 to 14, were produced by this approach. Many of these clusters were not observed in our previous work in which we used $Al_xH_y^-$ clusters to react with HMDS.[33] Two new LAl_n^- species, LAl_6^- and LAl_7^-, were selected for further analysis by carrying out anion photoelectron spectroscopy and density

[a] *Department of Chemistry, Johns Hopkins University, Baltimore, MD 21218, USA. E-mail: kbowen@jhu.edu*
[b] *Department of Physics & Engineering, West Chester University, West Chester, PA 19383, USA. E-mail: akandalam@wcupa.edu*
[c] *Department of Chemistry and Physics, McNeese State University, Lake Charles, LA 70609, USA*
† Present address: Advanced Bioimaging Center, Department of Molecular and Cell Biology, University of California, Berkeley.

functional theory (DFT) calculations. Agreement between the experimental and computational vertical detachment energies (VDEs) and adiabatic detachment energies (ADEs) validate the computed structures of these clusters.

Methods

Experimental

Anion photoelectron spectroscopy is conducted by crossing a beam of mass-selected negative ions with a fixed-frequency photon beam and energy-analyzing the resultant photo-detached electrons. The photo-detachment process is governed by the energy-conserving relationship: $h\nu$ = EBE + EKE, where $h\nu$ is the photon energy, EBE is the electron binding energy, and EKE is the electron kinetic energy. Our apparatus consists of a laser vaporization cluster anion source with an attached reaction cell, a time-of-flight mass spectrometer, a Nd:YAG photodetachment laser, and a magnetic bottle electron energy analyzer.[39] The photoelectron spectrometer resolution is $\sim$35 meV at 1 eV EKE. The third (355 nm) harmonic output of a Nd:YAG laser was used to photo-detach electrons from mass-selected LAl_n^- clusters. Photoelectron spectra were calibrated against the atomic transitions of atomic Cu^-.[40]

The LAl_n^- clusters were generated using a laser-vaporization/ligation cell source which has been recently applied in our lab for the studies of various molecular reactions.[41] Here, aluminum cluster anions Al_n^- were initially generated by laser vaporization of an aluminum rod. The resultant plasma was cooled with 100 psig of helium gas delivered by a pulsed valve. The resulting aluminum cluster anions then traveled through a reaction cell (4 mm diameter), where they mixed with HMDS vapor. The HMDS vapor was introduced into the reaction cell by a second pulsed valve, which was backed by 15 psig of helium gas. The resulting LAl_n^- anionic clusters were mass-analyzed by the time-of-flight mass spectrometer and their photoelectron spectra were recorded.

Computational

The lowest energy isomers of neutral and negatively charged LAl_n^- (n = 5–7) clusters were determined by carrying out density functional theory (DFT) based calculations using the Gaussian09 code.[42] The gradient-corrected exchange–correlation functional,[43] mPW1PW91 along with 6-311++G(3df,3pd) basis set was used to compute energies of the optimized structures. The accuracy and the reliability of mPW1PW91 functional in predicting the experimental results of Al_n^- clusters have been established in a previously reported theoretical study.[44] In the geometry optimization procedure, the energy convergence criterion was set to 10^{-9} Hartree, while the gradient was converged to 10^{-4} Hartree $Å^{-1}$. The vibrational frequencies of all the isomers reported here are positive, thus these isomers correspond to various minima on their corresponding potential energy surfaces.

The vertical detachment energies (VDE) and adiabatic detachment energies (ADE) obtained from the DFT calculations were compared with the corresponding measured values. The VDEs were calculated following the definition VDE = $E_2 - E_1$, where E_1 is the total energy of the anion and E_2 is the total energy of the neutral, both calculated at the anion's ground state geometry. For the anionic complex with multiplicity M, neutral species with multiplicities $M - 1$ and $M + 1$ were considered in the VDE calculation. The higher transition energies were calculated following the extended Koopmans' theorem,[45] in which a correction term δE, was added to the eigen values of the ground state anion. The correction term δE is defined by the equation $\delta E = E_1 - E_2 - \varepsilon_{HOMO}$, where E_1 and E_2 are the same as discussed above, and ε_{HOMO} is the eigenvalue of the highest occupied molecular orbital (HOMO) of the anion in its ground state. The adiabatic detachment energy (ADE) is calculated as the energy difference between the lowest energy isomer of the anion and structurally identical isomer (nearest local minimum) of its neutral counterpart. If ground state isomers of the anion and neutral clusters are not significantly different, then the calculated ADE value of the anionic cluster corresponds to the electron affinity (EA) of the corresponding neutral cluster.

Results and discussion

The mass spectra, with and without HMDS pulsed into the reaction cell, are shown in Fig. 1. With no HMDS in the reaction cell, bare aluminum cluster anions, Al_n^-, are observed in the mass spectrum; when HMDS is injected into the cell, a new series of ligated aluminum cluster anions LAl_n^- appears, where L is identified as deprotonated HMDS, *i.e.*, $N[Si(Me)_3]_2$. The size of the aluminum core in LAl_n^- ranges from 1 to 14, of which LAl_5^- to LAl_{14}^- have not been observed prior to the current work. This further demonstrates the capability of this laser vaporization–reaction cell setup in preparing various ligated metal cluster anions in the gas phase.[39]

Photoelectron spectra were recorded for three selected LAl_n^- species: LAl_4^-, LAl_6^- and LAl_7^-systems, and these are displayed

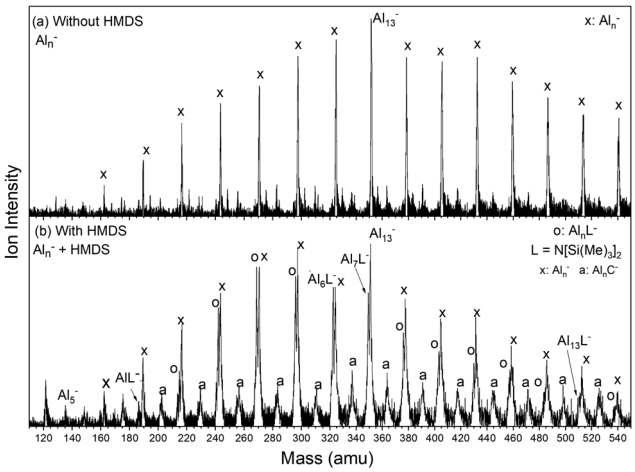

Fig. 1 Mass spectra of (a) bare aluminum cluster anions, Al_n^-, and (b) deprotonated HMDS-ligated aluminum cluster anions, LAl_n^- (L = $N[Si(Me)_3]_2$).

in Fig. 2. In an anion photoelectron spectrum, the electron binding energy (EBE) value at the peak position in the lowest EBE spectral feature is the vertical detachment energy (VDE), which corresponds to the photo-detachment transition at which the Franck–Condon overlap is maximal between the wave functions of the anion and its neutral counterpart. When there is sufficient Franck–Condon overlap between these two energy states, and when no vibrational hot bands are present, the EA value can be determined as the EBE value at the threshold of the lowest EBE band. Here, the EA values are assigned by extrapolating the low EBE side of the lowest EBE spectral feature to zero intensity.

The LAl_4^- spectrum was taken to compare with the previous LAl_4^- spectrum[33] as a cross-validation, and no significant difference between them can be observed. This demonstrates that the LAl_n^- made in the current work are the same species as those made previously, though they are prepared by reacting HMDS with different low OS aluminum precursors, *i.e.*, bare aluminum cluster anions *versus* aluminum hydride cluster anions. The photoelectron spectrum of LAl_6^- has a band between 2.2 eV to 3.2 eV, with the first EBE feature starting at about 2.2 eV with several close peaks ranging from 2.6 eV to 3.2 eV. The experimental EA of LAl_6 is taken to be 2.2 eV and the experimental VDE of LAl_6^- is 2.62 eV. In the spectrum of LAl_7^-, we observe that its lowest EBE band starts at approximately 1.9 eV and reaches maximal intensity at 2.34 eV. Therefore, the EA of neutral LAl_7 and the VDE of LAl_7^- are determined as 1.9 and 2.34 eV, respectively. The measured and calculated VDE and ADE values of these systems are given in Table 1.

Table 1 Experimentally measured ADE, VDE values and calculated ADE and VDE values. All numbers are in eV

Systems	Expt. ADE	Theo. ADE	Expt. VDE	Theo. VDE
LAl_5^-	—	2.00 (isomer **3a**)	—	2.18 (isomer **3a**)
		1.71 (isomer **3c**)		2.10 (isomer **3c**)
LAl_6^-	2.20	2.23 (isomer **5a**)	2.60	2.52 (isomer **5a**)
		2.20 (isomer **5b**)		2.40 (isomer **5b**)
LAl_7^-	1.90	1.96 (isomer **6a**)	2.34	2.64 (isomer **6a**)
		1.90 (isomer **6b**)		2.22 (isomer **6b**)

Even though photoelectron spectrum for LAl_5^- is not reported here, we carried out DFT based calculations and determined the lowest energy isomers of neutral and anionic LAl_5 systems (Fig. 3). For LAl_5^- cluster, our calculations reveal three nearly energetically-degenerate (within 0.20 eV) structures (Fig. 3a–c) competing to stabilize the cluster. In the lowest energy structure, isomer **3a**, the Al_5^- moiety forms a distorted triangular bi-pyramid with one of its Al atoms inserting between a Si–CH_3 bond of the ligand, while another Al atom, bound to the N atom of the ligand, L. This isomer can be considered as an extension of the lowest energy isomer of LAl_4^-, reported in our previous study.[33] In isomer **3b**, which is 0.15 eV higher in energy than isomer **3a**, the Al_5^- moiety forms a quasi-planar unit, where in one of the Al atoms is bound to the N atom while another Al atom is inserted into one of the Si–CH_3 bonds of the ligand, L. It is noteworthy here that the structure of Al_5^- moiety in **3b** is identical to the previously reported[44] structure of pure Al_5^- cluster. The Al_5^- moiety in the third anionic isomer of LAl_5^-, **3c** (ΔE = 0.16 eV), is also structurally similar to the pure Al_5^- cluster, albeit with a slight distortion due to its interaction with the ligand. However, unlike in the other isomers of LAl_5^-, in isomer **3c**, two Al atoms are inserted between the same Si–CH_3 bond of the ligand. This is the first instance among the LAl_n^- (n = 2–5) clusters, where two Al atoms are inserted between the same Si–CH_3 bond of the ligand. In addition, as we go from LAl_4^- to LAl_5^- cluster, these structures demonstrate a growth pattern where the additional Al atom prefers to bond to other Al atoms, instead of bonding with the ligand directly. All of these anionic isomers prefer a spin multiplicity of doublet ($2S$ + 1 = 2). The calculated VDE

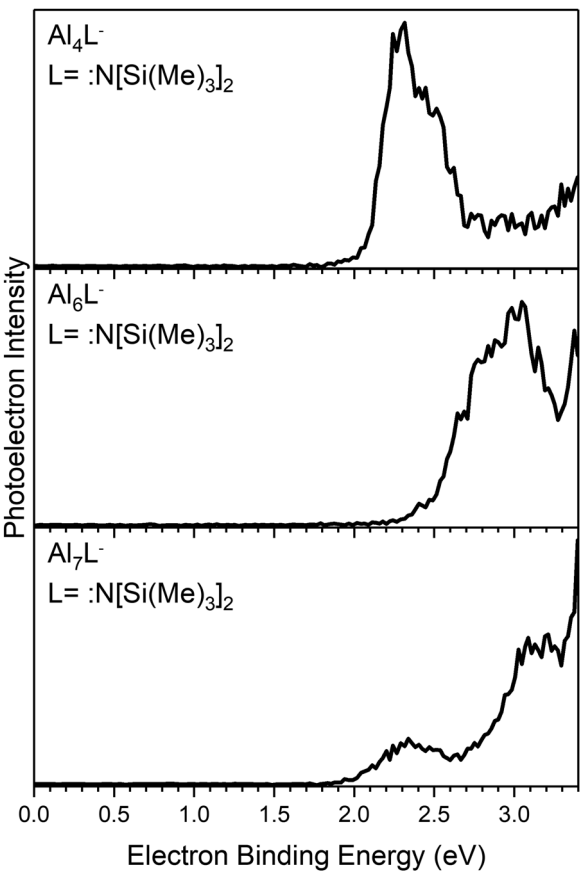

Fig. 2 Anion photoelectron spectra of LAl_4^-, LAl_6^-, and LAl_7^- (L = N[Si(Me)$_3$]$_2$), taken with the third harmonic (355 nm wavelength) of a Nd:YAG laser.

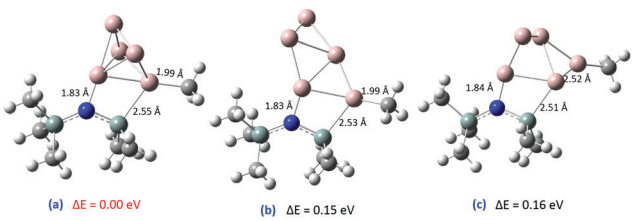

Fig. 3 The three lowest energy isomers of LAl_5^- cluster, where L = Ni[Si(CH$_3$)$_3$]$_2$. The relative energies are given in eV.

values of isomer **3a** are 2.18 eV (corresponding to transition from anionic doublet to neutral singlet) and 2.49 eV (transition from anionic doublet to neutral triplet). For isomer **3b**, wherein the Al_5^- moiety is similar to that of the pure Al_5^- cluster, the calculated VDE values are 2.49 (2 → 1) and 2.51 eV (2 → 3). The calculated VDE values of isomer **3c**, are 2.10 eV (2 → 1) and 2.40 eV (2 → 3). It is to be noted here that the measured VDE value of pure Al_5^- cluster was reported[46,47] to be 2.30 eV. Thus, the effect of ligand on the electron binding energy of the Al_5^- seems to be minimal.

The three lowest energy structures of neutral LAl_5 are given in Fig. 4(a–c). Isomer **4a**, the lowest energy isomer, consists of a quasi-planar Al_5 moiety interacting with the ligand, wherein two Al atoms are inserted between the Si–CH_3 bond, while a third Al atom is bound to the N-atom of the ligand, L. Note that this isomer is similar to isomer **3c**, the higher energy isomer of LAl_5^-. Isomer **4b**, which is just 0.12 eV higher in energy than isomer **4a**, consists of Al_5 moiety in the shape of distorted triangular bi-pyramid, with its Al atoms inserting between a Si–CH_3 bond, while another Al atom, bound to the N atom of the ligand. This isomer is structurally analogous to the lowest energy isomer of LAl_5^- (isomer **3a**). The calculated ADE value of isomer **3a**, calculated as the energy difference between isomer **3a** and its neutral analog, isomer **4b** is 2.00 eV; while the ADE value of isomer **3c**, calculated as the energy difference between isomer **3c** and isomer **4a** is 1.71 eV. Note that our calculations did not reveal a neutral analog of isomer **3b** as it was not a minimum on the potential energy surface of the neutral cluster.

The lowest energy isomers of anionic and neutral LAl_6 systems are given in Fig. 5. In the lowest energy isomer of anionic LAl_6^-, (isomer **5a**) two Al atoms of an Al_6^- octahedral moiety are inserted between a Si–CH_3 bond of the ligand, while another Al atom is bound to the N-atom of the ligand, L. The next higher energy isomer (ΔE = 0.63 eV), isomer **5b**, has only one Al atom of a slightly distorted Al_6^- octahedron inserted between a Si–CH_3 bond of the ligand. Note that the pure Al_6^- cluster also forms an octahedron structure.[44] Interestingly, a structure where two Al atoms of the Al_6^- moiety are inserted between two different Si–CH_3 bonds of the ligand is 0.88 eV higher in energy than isomer **5a**. In this higher energy isomer,

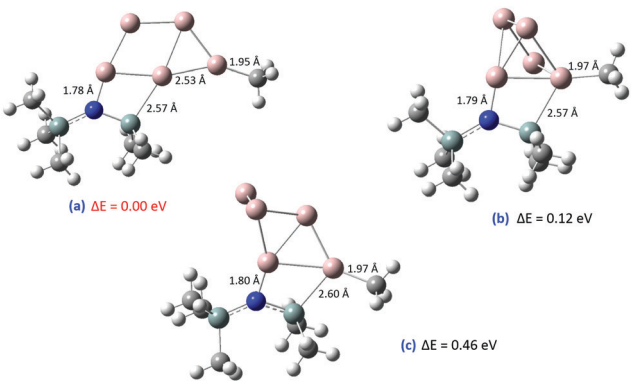

Fig. 4 The three lowest energy isomers of neutral LAl_5 cluster, where L = Ni[Si(CH_3)$_3$]$_2$. The relative energies are given in eV.

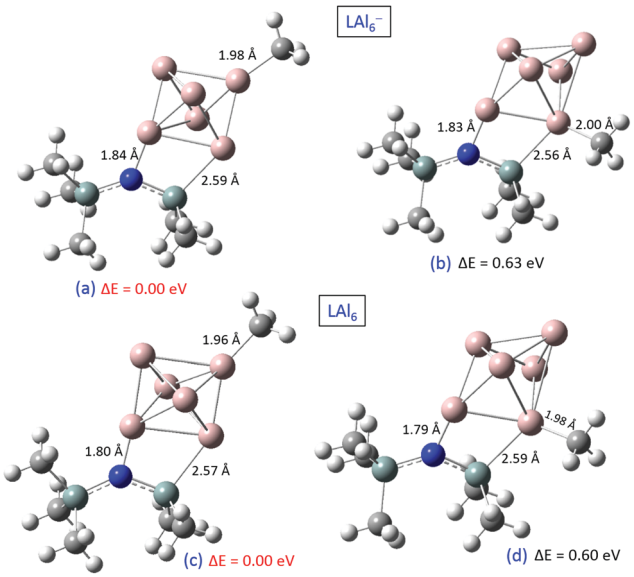

Fig. 5 The lowest energy isomers of negatively charged and neutral LAl_6 clusters, where L = Ni[Si(CH_3)$_3$]$_2$. The relative energies are given in eV.

the Al_6^- moiety adopted a planar geometry. In addition, the structure in which an Al_6^- octahedron is bound to just the N-atom of the ligand, without any Al insertions is 0.82 eV higher in energy than isomer **5a**. Our calculated VDE value of the lowest energy isomer (isomer **5a**) 2.52 eV, while the VDE of next higher energy isomer (isomer **5b**) is calculated to be 2.40 eV. Both these VDE values are in good agreement with the measured value of 2.6 eV. Note that the measured VDE value of pure Al_6^- was reported[46,47] as 2.63 ± 0.06 eV, again indicating that our ligand, L has a minimal effect on the electron binding energy of Al_6^-. This is consistent with the observation in our previous study[33] on LAl_n^- (n = 2–4) and in LAl_5^-. Since the photoelectron spectrum of LAl_6^- consists of a band made up of several peaks ranging from 2.6 to 3.1 eV and to understand how many isomers are contributing towards the first broad peak of the photoelectron spectrum, we calculated the higher transition energies of both the isomers (isomers **5a** and **5b**) by employing extended Koopman's theorem. The next two higher energy transitions are due to the electron detachments from HOMO−1 and HOMO−2, respectively. In the case of isomer **5a**, these higher transition energies are calculated to be 2.8 eV and 3.10 eV, while in the isomer **5b**, they are 2.70 eV and 3.31 eV. The calculated VDE values and the higher energy transitions of both isomers, **5a** and **5b**. Are in good agreement with the observed photoelectron spectra of LAl_6^-. Hence, we can report that both these isomers are present in the cluster beam of LAl_6^- and have contributed towards the photoelectron spectrum of LAl_6^- given in Fig. 2. However, since the energy of the isomer **5b** is 0.63 eV higher in energy than isomer **5a**, the concentration of isomer **5b** is expected to be significantly lower than that of isomer **5a**.

The lowest energy isomer of neutral LAl_6, isomer **5c**, is similar to that of its anionic counterpart, wherein two Al atoms of Al_6 octahedron are inserted between a Si–CH_3 bond of the

ligand, L. The next higher energy isomer (ΔE = 0.60 eV), isomer **5d**, is similar to isomer **5b**, the higher energy isomer of LAl_6^-. The calculated ADE value of isomer **5a** is 2.23 eV, while the ADE of isomer **5b** is 2.20 eV. Since the lowest energy isomers of anionic and neutral LAl_6 are identical, we can designate the ADE values of LAl_6^- as the EA of the neutral LAl_6. These two values are in excellent agreement with the measured value of 2.2 eV, thus reinforcing the contribution of both isomers in the photoelectron spectrum of LAl_6^-.

Fig. 6 shows the lowest energy isomers of negatively charged and neutral LAl_7 systems. Our calculations reveal two energetically nearly-degenerate (ΔE = 0.12 eV) structures for LAl_7^-, isomer **6a** and isomer **6b**. The lowest energy isomer of LAl_7^- (isomer **6a**), consists of a face-capped octahedral Al_7^- moiety, with two Al atoms inserted between the Si–CH_3 bond of the ligand and the face-capping Al atom bound to the N atom of the ligand, L. In the next higher energy isomer (isomer **6b**), the Al_7^- moiety forms a face-capped prism structure, with the Al atom capping the square face of the Al_6 prism bound to the N atom of the ligand. In addition, two Al atoms are inserted between the Si–CH_3 bond of the ligand. Both these anionic isomers prefer to form a doublet ($2S + 1 = 2$) spin state. The calculated VDE values of isomer **6a** are 2.64 eV (transition from anionic doublet to neutral singlet) and 2.91 eV (transition from anionic doublet to neutral singlet), while the VDE values of isomer **6b** are calculated to be 2.22 eV (2 → 1) and 2.87 eV (2 → 3). Comparing our calculated lowest energy electron detachment values (for transition from anionic doublet to neutral singlet states) of both these isomers with the photoelectron spectrum of LAl_7^- given in Fig. 2, we can say that both isomers are contributing towards the lowest EBE band, which is a result of an overlap of two peaks, one centered around 2.20 eV and the other centered around 2.40 eV. The next higher energy EBE band of the spectrum (see Fig. 2) starts around 2.7 eV and extends to 3.4 eV. Our calculated electron detachment energy values, corresponding to transitions from anionic doublet to neutral triplet states in both isomers (2.91 and 2.87 eV) are contributing towards this higher energy band. In addition, we have also calculated other higher transition energies using the extended Koopman's theorem. For isomer **6a**, the next three transition energies are 3.00, 3.12, and 3.27 eV; for isomer **6b**, they are 3.00, 3.18, and 3.26 eV. These transitions are all in good agreement with the higher energy EBE band of the LAl_7^- spectrum given in Fig. 2. Thus, one can conclude that both isomers **6a** and **6b** are present in the cluster beam and are contributing towards the photoelectron spectrum of LAl_7^-. It is to be noted here that the measured VDE value of pure Al_7^- cluster was reported[46,47] to be 2.30 eV. Thus, the effect of ligand on the electron binding energy of the Al_7^- seems to be minimal.

The lowest energy isomer of neutral LAl_7 (isomer **6c**) also consists of a face-capped Al_7 octahedron, with two of its Al atoms inserted between the Si–CH_3 bond. Unlike in the case of the anionic lowest energy isomer (isomer **6a**), in this isomer the face-capping Al atom is bound to the methyl group of the ligand. The next higher energy isomer (isomer **6d**) corresponds to a face-capped Al_7 octahedron, but with only one Al atom inserted between the Si–CH_3 bond. This single-atom inserted isomer (isomer **6d**) is 0.80 eV higher in energy than "two-atom" inserted isomer (isomer **6c**). The calculated ADE value of isomer **6a** is 1.96 eV, which is in good agreement with the experimental ADE value of 1.90 eV.

Having established the ground state isomers of neutral and anionic LAl_n systems, we now turn to understand the interesting structural features of these systems. The ground state structures of neutral and anionic LAl_n (n = 2–7) systems can be viewed as a result of the activation of Si–CH_3 bond and subsequent migration of the methyl group to the rest of the metal cluster. In our earlier reported study,[33] it was observed that as we move from LAl_2^- to LAl_4^-, the energy difference between the isomer with an Al-atom inserted into the Si–CH_3 bond and the isomer without any breaking of Si–CH_3 bond, increased from 0.50 eV to 0.68 eV. This clearly indicates an increased preference for structures in which the methyl group of the ligand has migrated to one of the Al atoms of the metal cluster thereby resulting in an Al-atom insertion between Si–CH_3. In the current study, as we move from LAl_5^- to LAl_7^-, a clear preference for structures with two Al atoms inserted between the Si–CH_3 bond (see Fig. 3, 5 and 6) emerges. As the aluminum cluster size increased from Al_5 to Al_7, a single-aluminum atom insertion into Si–CH_3 bond has resulted in destabilizing the structural integrity and electron delocalization in the metal cluster (see Fig. 5b and d). Thus, to maintain the structural integrity and delocalization, the methyl group further migrated to another Al atom of the Al_n cluster, thereby resulting in a more symmetric Al_n^- moiety (see Fig. 5a and c). This migration has resulted in a more stable structure, which was labeled as "two-atom" inserted isomers.

The four frontier molecular orbitals (MOs) of LAl_n^- (n = 5–7) are given in Fig. 7. If one considers the LAl_n^- complex as a ligand, L interacting with an aluminum cluster, then the bonding and the molecular orbital composition becomes clear.

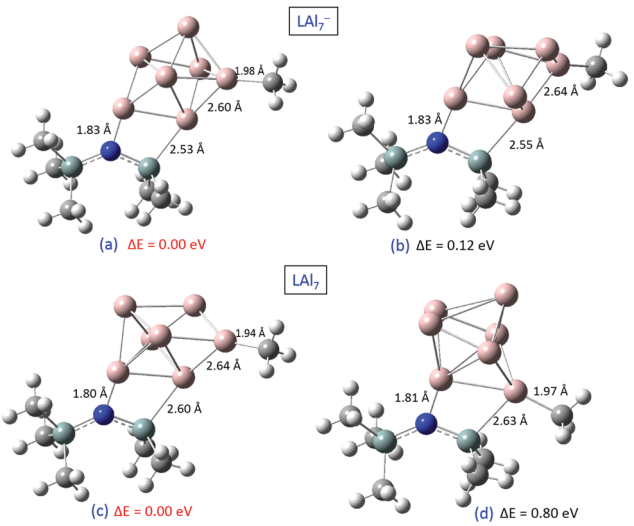

Fig. 6 The lowest energy isomers of negatively charged and neutral LAl_7 clusters, where L = $Ni[Si(CH_3)_3]_2$. The relative energies are given in eV.

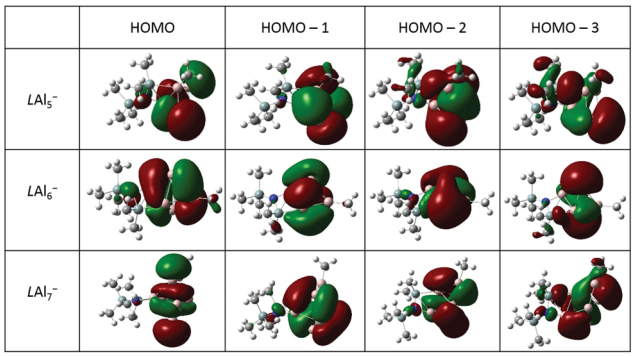

Fig. 7 The four frontier molecular orbitals of LAl_n^- (n = 5–7), where L = $Ni[Si(CH_3)_3]_2$.

The frontier bonding orbitals for all the complexes considered here show bonding interactions between the Al atoms in the metal cluster with negligible contributions from the ligand. This is fairly obvious due to the weak bonding between Al–Al atoms in these small cluster range. Since the MO picture show a delocalized bonding pattern within the aluminum cluster, one would anticipate minimal disturbance to bonds as an electron is removed from these MOs with each transition in the photoelectron spectroscopy. NPA charge analysis provides further insight into the nature of these complexes. The charge on the Al_n cluster in the anionic complexes is very small, indicating that the negative charge is mostly located on the ligand. A comparison of the NPA charges on the anionic and neutral LAl_n complexes revealed that during the photo-detachment of the extra electron from the anionic LAl_n^-, it is the Al_n moiety that lost majority (>80%) of the charge. Note that a similar pattern was reported in our previous study[33] on LAl_n (n = 2–4) complexes.

Concluding remarks

A wide range of low-oxidation state aluminum-containing clusters, LAl_n^- (n = 1–14), were generated *via* the direct reaction between bare aluminum cluster anions and the hexamethyldisilazane molecules. Among them, the geometrical and electronic structure of LAl_6^- and LAl_7^- systems were characterized by using negative ion photoelectron spectroscopy and density functional theory-based calculations. Our computational results show that as the size of the aluminum cluster increased from n = 5 to 7, a CH_3-group from the ligand migrated onto the aluminum metal cluster, thus forming structures in which two Al atoms are inserted between Si–CH_3 bond. The effect of the ligand on the geometrical and electronic structure of Al_n moiety seems to be minimal, with the Al_n retaining its structural integrity during the interaction with the ligand and the calculated (and measured) electron detachment energies similar to that of the pure Al_n^- clusters.

Conflicts of interest

There are no conflicts to declare.

Acknowledgements

This material is based on work supported by the Office of Naval Research (ONR), Multidisciplinary University Research Initiative (MURI) under Grant No. N00014-15-1-2681 and the Air Force Office of Scientific Research (AFOSR) under Grant No. FA9550-19-1-0077 (K. H. B.).

References

1 W. Roesky and S. S. Kumar, *Chem. Commun.*, 2005, 4027–4038.
2 H. W. Roesky, *Inorg. Chem.*, 2004, **43**, 7284–7293.
3 M. Tacke and H. Schnöckel, *Inorg. Chem.*, 1989, **28**, 2895–2896.
4 M. Mocker, C. Rob and H. Schnöckel, *Angew. Chem.*, 1994, **106**, 1860–1861.
5 A. Ecker and H. Schnöckel, *Z. Anorg. Allg. Chem.*, 1996, **622**, 149–152.
6 C. Dohmeier, C. Roble, M. Tacke and H. Schnöckel, *Angew. Chem.*, 1991, **103**, 594–595.
7 C. Dohmeier, D. Loos and H. Schnöckel, *Angew. Chem.*, 1996, **108**, 141–161.
8 J. Gauss, U. Schneider, R. Ahlrichs, C. Dohmeier and H. Schnöckel, *J. Am. Chem. Soc.*, 1993, **115**, 2402–2408.
9 A. Purath, R. Köppe and H. Schnöckel, *Angew. Chem.*, 1999, **111**, 3114–3116Angew. Chem. Int. Ed., 1999, 38, 2926.
10 A. Purath, R. Köppe and H. Schnöckel, *Chem. Commun.*, 1999, 1933–1934.
11 H. Köhnlein, A. Purath, C. Klemp, E. Baum, I. Krossing, G. Stösser and H. Schnöckel, *Inorg. Chem.*, 2001, **40**, 4830–4838.
12 E. Ecker, E. Weckert and H. Schnöckel, *Nature*, 1997, **387**, 379–381.
13 C. Dohmeier, M. Mocker, H. Schnöckel, A. Lötz, U. Schneider and R. Ahlrichs, *Angew. Chem.*, 1993, **105**, 1491–1493 (*Angew. Chem. Int. Ed.*, 1993, **32**, 1428).
14 A. Schnepf and H. Schnöckel, *Adv. Organomet. Chem.*, 2001, **47**, 235–281.
15 C. Üffing, A. Ecker, R. Köppe, K. Merzweiler and H. Schnöckel, *Chem. – Eur. J.*, 1998, **4**, 2142–2147.
16 N. Etkin and D. W. Stephan, *Organometallics*, 1998, **17**, 763–765.
17 S. J. Urwin, D. M. Rogers, G. S. Nichol and M. J. Cowley, *Dalton Trans.*, 2016, **45**, 13695–13699.
18 A. Haaland, K.-G. Martinsen, S. A. Shlykov, H. V. Volden, C. Dohmeier and H. Schnöckel, *Organometallics*, 1995, **14**, 3116–3119.
19 J. D. Gorden, A. Voigt, C. L. B. Macdonald, J. S. Silverman and A. H. Cowley, *J. Am. Chem. Soc.*, 2000, **122**, 950–951.
20 C. Dohmeier, H. Krautscheid and H. Schnöckel, *Angew. Chem.*, 1994, **106**, 2570–2572.
21 C. Üffing, A. Ecker, R. Köppe and H. Schnöckel, *Organometallics*, 1998, **35**, 2373–2375.
22 Q. Yu, A. Purat, A. Douchev and H. Schnöckel, *J. Organomet. Chem.*, 1999, **584**, 94.

23 J. Weiß, D. Stetzkamp, B. Nuber, R. A. Fischer, C. Boehme and G. Frenking, *Angew. Chem., Int. Ed. Engl.*, 1997, **36**, 70–72.
24 D. Weiß, T. Steinke, M. Winter, R. A. Fischer, N. Fröhlich, J. Uddin and G. Frenking, *Organometallics*, 2000, **19**, 4583–4588.
25 S. Schulz, T. Schoop, H. W. Roesky, L. Häming, A. Steiner and R. Herbst-Irmer, *Angew. Chem., Int. Ed. Engl.*, 1995, **34**, 919–920.
26 C. K. F. von Haenish, C. Üffing, M. A. Junker, A. Ecker, B. O. Kneisel and H. Schnöckel, *Angew. Chem., Int. Ed. Engl.*, 1996, **35**, 2875–2877.
27 C. Dohmeier, H. Schnöckel, C. Robl, U. Schneider and R. Ahlrichs, *Angew. Chem., Int. Ed. Engl.*, 1994, **33**, 199–200.
28 C. Ganesamoorthy, S. Loerke, C. Gemel, P. Jerabek, M. Winter, G. Frenking and R. A. Fischer, *Chem. Commun.*, 2013, **49**, 2858–2860.
29 J. Vollet, J. R. Hartig and H. Schnöckel, *Angew. Chem., Int. Ed.*, 2004, **43**, 3186–3189.
30 K. Weiß and H. Schnöckel, *Anal. Bioanal. Chem.*, 2003, **377**, 1098.
31 K. S. Williams and J. P. Hooper, *J. Phys. Chem. A*, 2011, **115**, 14100–14109.
32 X. Zhang, G. Gantefoer, B. Eichhorn, D. Mayo, W. H. Sawyer, A. F. Gill, A. K. Kandalam, H. Schnöckel and K. Bowen, *J. Chem. Phys.*, 2016, **145**, 074305.
33 X. Zhang, L. Wang, G. Montone, A. Gill, G. Gantefoer, B. Eichhorn, A. K. Kandalam and K. H. Bowen, *Phys. Chem. Chem. Phys.*, 2017, **19**, 15541–15548.
34 X. Zhang, G. Liu, G. Gantefoer, K. H. Bowen and A. N. Alexandrova, *J. Phys. Chem. Lett.*, 2014, **5**, 1596–1601.
35 (*a*) X. Zhang, G. Liu, K.-H. Meiwes-Broer, G. Ganteför and K. H. Bowen, *Angew. Chem., Int. Ed.*, 2016, **55**, 9644–9647; (*b*) G. Liu, P. Poths, X. Zhang, Z. Zhu, M. Marshall, M. Blankenhorn, A. N. Alexandrova and K. H. Bowen, *J. Am. Chem. Soc.*, 2020, **142**, 7930–7936.
36 X. Li, H. Wu, X.-B. Wang and L.-S. Wang, *Phys. Rev. Lett.*, 1998, **81**, 1909–1912.
37 C. Y. Cha, G. Gantefor and W. Eberhardt, *J. Chem. Phys.*, 1994, **100**, 995–1010.
38 S. R. Miller, N. E. Schultz, D. G. Truhlar and D. G. Leopold, *J. Chem. Phys.*, 2009, **130**, 024304.
39 G. Liu, S. Ciborowski and K. H. Bowen, *J. Phys. Chem. A*, 2017, **121**, 5817–5822.
40 J. Ho, K. M. Ervin and W. C. Lineberger, *J. Chem. Phys.*, 1990, **93**, 6987.
41 (*a*) G. Liu, E. Miliordos, S. M. Ciborowski, M. Tschurl, U. Bosel, U. Heiz, X. Zhang, S. S. Xantheas and K. H. Bowen, *J. Chem. Phys.*, 2018, **149**, 221101; (*b*) G. Liu, S. M. Ciborowski, Z. Zhu, Y. Chen, X. Zhang and K. H. Bowen, *Phys. Chem. Chem. Phys.*, 2019, **21**, 10955–10960; (*c*) G. Liu, Z. Zhu, S. M. Ciborowski, I. R. Ariyarathna, E. Miliordos and K. H. Bowen, *Angew. Chem., Int. Ed.*, 2019, **121**, 7855–7859; (*d*) G. Liu, I. R. Ariyarathna, S. M. Ciborowski, Z. Zhu, E. Miliordos and K. H. Bowen, *J. Am. Chem. Soc.*, 2020, **142**(51), 21556–21561.
42 M. J. Frisch, G. W. Trucks and H. B. Schlegel, *et al.*, *GAUSSIAN09, Revision B.01*, Gaussian, Inc., Wallingford, CT, 2004.
43 C. Adamo and V. Baron, *J. Chem. Phys.*, 1998, **108**, 664–675; J. P. Perdew, *Electronic Structure of Solids*, Akademic Verlag, Berlin, Germany, 1991.
44 S. Paranthaman, K. Hong, J. Kim, D. E. Kim and T. K. Kim, *J. Phys. Chem. A*, 2013, **117**, 9293–9303.
45 D. J. Tozer and N. C. Handy, *J. Chem. Phys.*, 1998, **109**, 10180.
46 X. Li, H. Wu, X.-B. Wang and L.-S. Wang, *Phys. Rev. Lett.*, 1998, **81**, 1909–1912.
47 C. Y. Cha, G. Gantefor and W. Eberhardt, *J. Chem. Phys.*, 1994, **100**, 995–1010.